Hindawi
Journal of Nanomaterials
Volume 2017, Article ID 7901686, 10 pages
https://doi.org/10.1155/2017/7901686

Research Article

Reaction and Characterization of Low-Temperature Effect of Transition Nanostructure Metal Codoped SCR Catalyst

Ke Yang,[1] Weiwei Xiao,[1] Quan Xu,[1] Jiaojiao Bai,[2] Yan Luo,[3] Hao Guo,[4] Li Cao,[1] Wei Cai,[1] Peng Pu,[1] and Lulu Cai[2]

[1] *State Key Laboratory of Heavy Oil Processing, Beijing Key Laboratory of Biogas Upgrading Utilization, China University of Petroleum, Beijing 102249, China*
[2] *Personalized Drug Therapy Key Laboratory of Sichuan Province, Hospital of the University of Electronic Science and Technology of China and Sichuan Provincial, People's Hospital, Chengdu 610072, China*
[3] *Department of Chemical Engineering, West Virginia University, Morgantown, WV 26505, USA*
[4] *Chongqing Institute of Forensic Science, Chongqing 400021, China*

Correspondence should be addressed to Quan Xu; xuquan@cup.edu.cn, Peng Pu; pupeng@hotmail.fr, and Lulu Cai; lzxlulu@126.com

Received 24 January 2017; Accepted 28 February 2017; Published 20 September 2017

Academic Editor: Jinwei Gao

Typical p-type semiconductor MnOx codoped with n-type semiconductors such as CeO_2 and V_2O_5 was reported to achieve high efficiency in catalytic NOx removal by NH_3. In this paper, we present novel Mn-Ce codoped V_2O_5/TiO_2 catalyst which exhibited an excellent NO conversion efficiency of 90% at 140°C. By using this codoped catalyst, the best low-temperature activity was greatly decreased when compared with single Mn- or Ce-doped catalyst. According to the characterization results from BET, XRD, and XPS, the codoped catalyst was composed of both CeO_2 and amorphous Mn. The electron circulation formed between doping elements is believed to promote the electron transfer, which may be one of the reasons for excellent low-temperature denitration performance.

1. Introduction

NOx is mainly derived from industrial emissions, traffic emissions, and living emissions. NOx gases react to form smog and acid rain as well as being central to the formation of tropospheric ozone. It especially can form small solid particles through the secondary chemical reactions that cause serious pollutions to the environment. Therefore, it is necessary to take a denitration treatment for flue gas after combustion. Selective catalytic reduction is the most widely used and effective methods for the removal of NOx in industrial at present. The main two reactions are presented in the following:

$$\begin{aligned} 4NO + 4NH_3 + O_2 &\longrightarrow 4N_2 + 6H_2O \\ 2NO_2 + 4NH_3 + O_2 &\longrightarrow 3N_2 + 6H_2O \end{aligned} \quad (1)$$

NH_3 and NO almost do not react in the absence of the catalyst; therefore, the catalyst is the key for the whole reaction. V_2O_5/TiO_2 and V_2O_5-WO_3/TiO_2 (anatase) catalysts operated at 350–400°C, with less than 1% V_2O_5 loading, have been widely accepted as commercial catalysts [1–3]. Currently, other doped companions such as Mn, Cu, Fe, Ce, Wo, and F [4–8] and morphological changes in the supports can be used to modify the catalyst to achieve high catalytic activity [9–12]. W or Mo doped V_2O_5/TiO_2, considered as the most effective commercial catalyst, is widely used for denitration in power plants and nitric acid plants [13, 14]. However, its narrow activity temperature window forces the selective catalytic reduction (SCR) unit to be installed upstream of the desulfurizer and electrostatic precipitator where high concentrations of SO_2 and particle matters can make the catalyst bed layer blocked, accelerating the deactivation of the catalyst [15]. Therefore, there is a rising interest in high

performance catalysts that can be used at low temperature. MnOx has attracted significant attention because of its various types of labile oxygen species [16, 17]. Recently, Ce-doped catalyst has been found to reduce the reaction temperature significantly and has high catalytic activity and selectivity [18]. Mn-doped catalyst has shown excellent low-temperature activity, lower apparent active energy, and better ion dispersion than those of most previously reported SCR catalysts [17, 19]. This research committed to the development of low-temperature catalyst based on the V_2O_5/TiO_2 and V_2O_5-CeO_2/TiO_2 catalyst, which is the key of the selective catalytic reduction (SCR) to remove NOx from effluent gas.

2. Materials and Methods

2.1. Materials. The low-temperature catalysts in the experiments were prepared with commercial anatase TiO_2 (Tianjin Guangfu Pharmaceutical) as carriers, with a specific surface area of 7.03 m^2/g. Ammonium metavanadate (NH_4VO_3) was used as the precursor of vanadium, cerium nitrate ($Ce(NO_3)_3{\cdot}6H_2O$) as the precursor of cerium, and oxalic acid solution as the precursor impregnation solution in the doping process. Manganese acetate ($C_4H_6MnO_{4.4}H_2O$), copper nitrate ($Cu(NO_3)_{2.3}H_2O$), cobalt nitrate ($Co(NO_3)_{2.6}H_2O$), ferric nitrate ($Fe(NO_3)_{3.9}H_2O$), and chromium nitrate ($Cr(NO_3)_{3.9}H_2O$) were selected to provide Mn, Cu, Co, Fe, and Cr, respectively. All these salts precursors were purchased from Tianjin Guangfu Technology Development Co., Ltd. and Aladdin Technology Co., Ltd.

2.2. Catalyst Preparation. The catalysts with different loadings of vanadium and cerium in the experiment were prepared by a conventional incipient-wetness impregnation method. Firstly, the oxalic acid was dissolved in deionized water and heated to dissolve completely, used as the precursor impregnation solution. Then, a certain quality of ammonium metavanadate was added to the oxalic acid solution and stirred until dissolved completely. A quantitative powder of cerium nitrate was added in the same way, finally, adding the TiO_2 powder to the above solution, stirring, and impregnating for 1 hour. The water was evaporated from the solution by a rotary evaporator and dried at 80°C for 24 hours. The dried samples were calcined at 500°C under the air atmosphere for 2 hours. Then the catalysts were ground and sieved to 20–40 mesh for catalytic performance evaluation. Other metals like Mn, Fe, Cr, etc. were doped in the same way as described above. Eventually, Ce-V_2O_5/TiO_2 catalyst with a fixed amount of 5% (wt%) V_2O_5 but different Ce loadings of 5%, 10%, 15%, 20%, 25%, and 30% (wt%) and other Bimetallic-doped V_2O_5/TiO_2 catalysts were prepared by the same impregnation method [20–22]. The catalysts prepared are denoted as xM-yCe-5V_2O_5/TiO_2. M represents the second metal, such as Mn, Fe, or Cu; x and y represent the loading of M (wt%) and Ce (wt%), respectively.

2.3. Catalytic Activity Test. The SCR activity measurement was performed on a fixed-bed stainless steel tube reactor with an inner diameter of 11 mm and the outer diameter of 14 mm. Laboratory gas distribution was used to simulate the flue gas in the measurement. The feed gas mixture consisted of NH_3 500 ppm, NO 500 ppm, 3% O_2 (volume fraction), and N_2 as the balance gas. The total flow rate was 1000 mL/min controlled by mass flow meters and the GHSV = 10,000 h^{-1} in each reaction. The concentrations of NOx were measured at the inlet and outlet by flue gas analyzer to calculate the conversion rate by the following:

$$\text{NO}x \text{ cpnversion (\%)} = \frac{[\text{NO}x]\text{ in} - [\text{NO}x]\text{ out}}{[\text{NO}x]\text{ in}} \times 100\%, \quad (2)$$

where $[\text{NO}x] = [\text{NO}] + [\text{NO}_2]$ and the in and out indicated the inlet and outlet concentration at steady state, respectively. The data was measured when the reaction reached the steady state (about 20–40 min) at each temperature, which could reduce the errors caused by instability.

2.4. Catalyst Characterization. The powder X-ray diffraction (XRD) measurements of the samples were recorded on a Bruker D8-Advance X-ray powder diffractometer using Cu Kα radiation (λ = 1.5406 Å) with scattering angles (2θ) of 5–85° and a 0.0197 step size. The specific surface areas and pore size were measured by nitrogen adsorption at −196°C by the BET method using Micromeritics ASAP 2020 M surface areas and porosity analyzer. The samples were degassed at 200°C for 12 hours. The X-ray photoelectron spectroscopy (XPS) experiments were carried out on a Thermo Fisher Escalab 250Xi X-ray photoelectron spectrometer system equipped with a monochromatic Al Kα X-ray source scanning from 0 to 5000 eV.

3. Results

3.1. Ce-Doped Effect of V_2O_5-TiO_2 Catalysts. NOx conversions rate at various temperatures for the NH_3-SCR over Ce-doped V_2O_5/TiO_2 catalysts is shown in Figure 1. V_2O_5/TiO_2 shows above 80% NOx conversion rate at a wide temperature range of 175°C to 375°C. The Ce doping can improve the catalytic activity effectively, especially from 160 to 450°C, due to the enhancement of electron transfer rate in catalyst. The 30Ce-V_2O_5/TiO_2 shows the highest NOx conversion and widest temperature window with NOx conversion above 90% from 160 to 400°C and the conversion rate could reach 99.83% at 200°C.

The catalytic activity with various Ce contents is shown in Figure 2. With the increase of Ce doping amount, the NOx conversion firstly decreased and then increased at low-temperature zone (100–200°C) and high-temperature zone (350–450°C). 10Ce-5V_2O_5/TiO_2 shows the worst catalytic activity, the NOx conversion even lower than the undoped 5V_2O_5/TiO_2 catalyst.

3.2. Low-Temperature Activity of X-Ce Codoped V_2O_5-TiO_2 Catalysts. Bimetal doped V_2O_5/TiO_2 catalyst was prepared on the basis of single Ce-doped catalyst. The Ce loadings were selected as 30 wt% based on the previous results and the cometal (Mn, Fe, Co, Cu, and Cr) loadings were varied

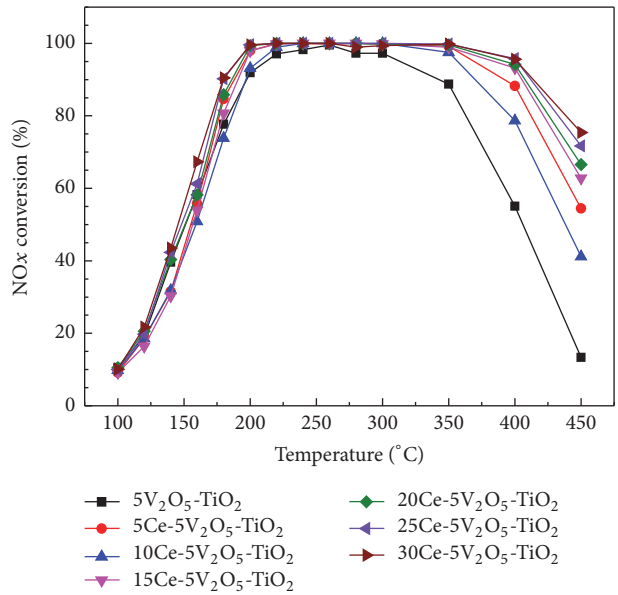

Figure 1: NOx conversion over Ce-doped V_2O_5/TiO_2 catalysts with different Ce contents.

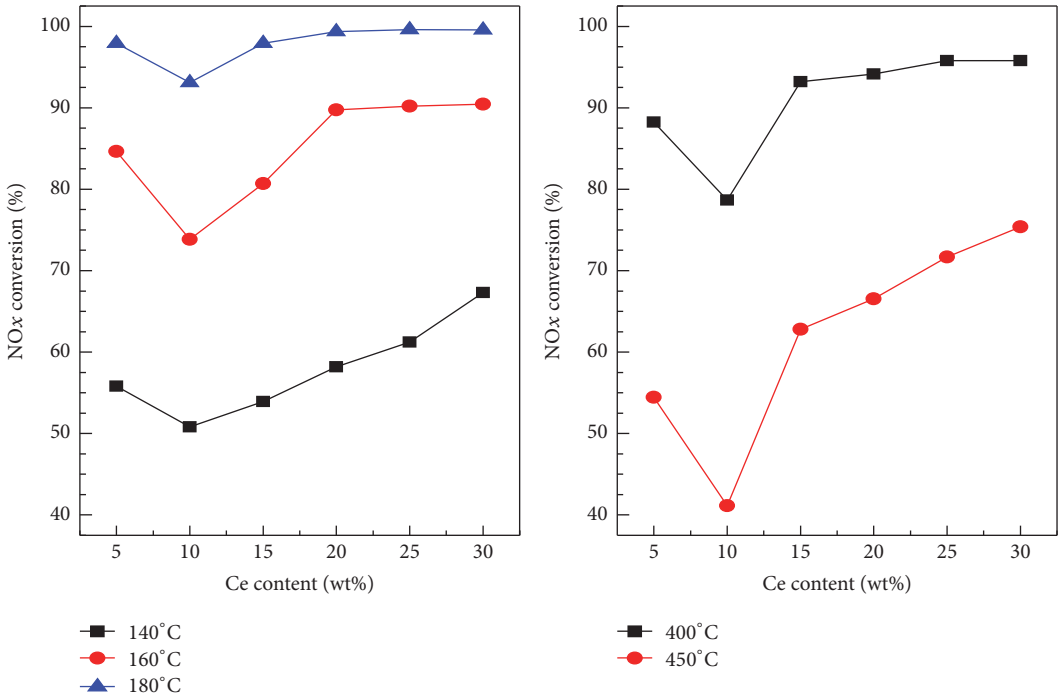

Figure 2: Effects of different Ce contents on NOx conversion.

ranging from 10 to 30 wt%. The catalytic activity was tested on the fixed-bed reactor at different temperatures, and the results are shown in Figures 3 and 4. From the results we can observe that the catalytic effect of Fe-Ce codoped catalyst is slightly lower than single Ce-doped catalyst at the low-temperature zone. The Cu-Ce codoped catalyst shows the worst activity, even less than the based V_2O_5/TiO_2 catalyst. Co-Ce and Cr-Ce codoped catalyst can improve the catalytic activity at the low-temperature zone but drop rapidly at high-temperatures zone. With a narrower active temperature window that cannot keep higher catalytic efficiency in a certain temperature range, Mn-Ce codoped V_2O_5/TiO_2 catalyst can improve the activity at low temperature effectively. It shows the best catalytic effect at low temperatures; the NOx conversion can reach 95.69% at 140°C. The 20Mn-30Ce-V_2O_5/TiO_2 catalyst is the best as the effect of 20Mn-30Ce-V_2O_5/TiO_2 and 30Mn-30Ce-V_2O_5/TiO_2 is almost similar.

The NOx conversion over X-Ce codoped V_2O_5/TiO_2 catalysts with loading contents of 20% at 160°C is shown in Figure 5. 20Mn-30Ce-V_2O_5/TiO_2 catalyst shows the best

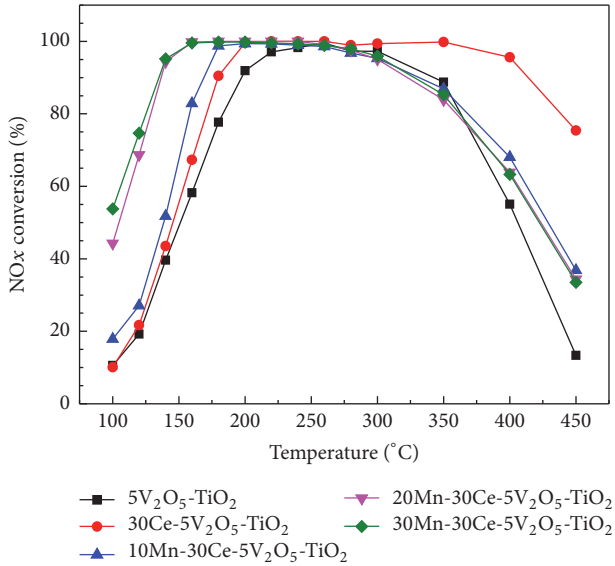

FIGURE 3: NOx conversion over Mn-Ce-V_2O_5/TiO_2 catalysts with different Mn contents.

activity that the conversion rate can reach 99.58% which is nearly 30% higher than singer Ce-doped. The catalytic activity over X-Ce codoped V_2O_5/TiO_2 catalysts is in the order of Mn-Ce > Co-Ce > Cr-Ce > Ce > Fe-Ce > Cu-Ce codoped.

3.3. Mn-Ce Codoped Effect. Initially, the single Mn- and Ce-doped V_2O_5/TiO_2 catalysts are prepared by the impregnation method to investigate the effect of single Mn or Ce, as compared to the Mn-Ce codoped catalyst. The result is shown in Figure 6. The NOx conversion over Mn-Ce codoped V_2O_5/TiO_2 catalyst can reach more than 90% at 140°C, which is much higher than single doped catalyst. Mn-Ce codoped V_2O_5/TiO_2 catalysts have the best low-temperature activity that can drop to 80°C which is lower than Mn-doped catalyst and Ce-doped catalyst. However, the catalytic activity is difficult to maintain at high temperature. Single Ce-doped catalyst has the widest temperature window, but the low-temperature effect is not obvious. Mn-doped catalyst has neither good low-temperature activity nor wide temperature window. Relevant characterizations have been taken to the three kinds of catalysts in this experiment.

3.4. XRD. The X-ray powder diffraction patterns of the Mn-Ce codoped and single Ce- and Mn-doped V_2O_5/TiO_2 catalysts are shown in Figure 7. All the reflections provide typical diffraction patterns for the TiO_2 anatase phase. The characteristic peaks of Ce and Mn oxides appear, respectively, in single Ce- and Mn-doped catalyst. In the pattern of 30Ce-V_2O_5/TiO_2, the doped Ce exists mainly in the form of CeO_2 and part of $CeVO_4$. It was found that CeO_2 can effectively improve the catalytic activity and make the reaction temperature window wider [18]. However, the formation of $CeVO_4$ has a certain suppression to the improvement of catalytic activity [23]. A variety of diffraction peaks of Mn oxides appeared in the single Mn-doped catalyst, including Mn_2O_3, Mn_3O_4, and MnO_2. With the codoping of Mn-Ce, the diffraction peaks of TiO_2 become weak significantly and CeO_2 crystal phase appears, but much weaker than single Ce-doped catalyst. The XRD results show that Mn, Ce, and TiO_2 have displayed a mutual influence by the codoping of Mn-Ce. The incorporation of Mn makes Ce exist in the form of CeO_2, but Mn is mostly in the amorphous state which can achieve a better low-temperature effect.

3.5. BET. The results of BET surface area, pore volume, and average pore diameter of each catalyst are shown in Table 1. Ce has a large particle diameter that the incorporation of Ce can improve the BET surface area effectively which is nearly five times more than original V_2O_5-TiO_2. Only a slight increase of the BET surface area has been achieved by the incorporation of Mn. But Mn-Ce codoped catalyst has the maximum surface area and minimum pore size. The change of BET surface area is consistent with the catalytic performance evaluation results in Figure 6.

3.6. XPS. The XPS spectra of Ce 3d of Mn-Ce codoped and single Ce-doped V_2O_5/TiO_2 catalyst are shown in Figure 8. The spectrum of Ce 3d contains eight peaks, in which u, u'', u''', v, v'', and v''' are the characteristic peaks of Ce^{4+} and u' and v' are the characteristic peaks of Ce^{3+}. According to the intensity of the peak, Ce mainly exists as Ce^{4+} in both Mn-Ce codoped and single Ce-doped catalyst. The incorporation of Mn impacts the surface valence distribution of Ce that the Ce^{4+} increases significantly and Ce^{3+} reduces accordingly. The relative surface concentration of Ce^{4+} and Ce^{3+} calculated by the peak area is shown in Figure 9. The ratio of $Ce^{4+}/(Ce^{3+} + Ce^{4+})$ increased from 85% to 88.87% for Ce-V_2O_5/TiO_2 and Mn-doped Ce-V_2O_5/TiO_2 catalysts, respectively. These results suggest that the incorporation of Mn can convert part of the Ce^{3+} Ce^{4+} and increase the proportion of Ce^{4+}.

The XPS spectra of Mn 2p of Mn-Ce codoped and single Mn-doped V_2O_5/TiO_2 catalyst are shown in Figure 10. Mn 2p

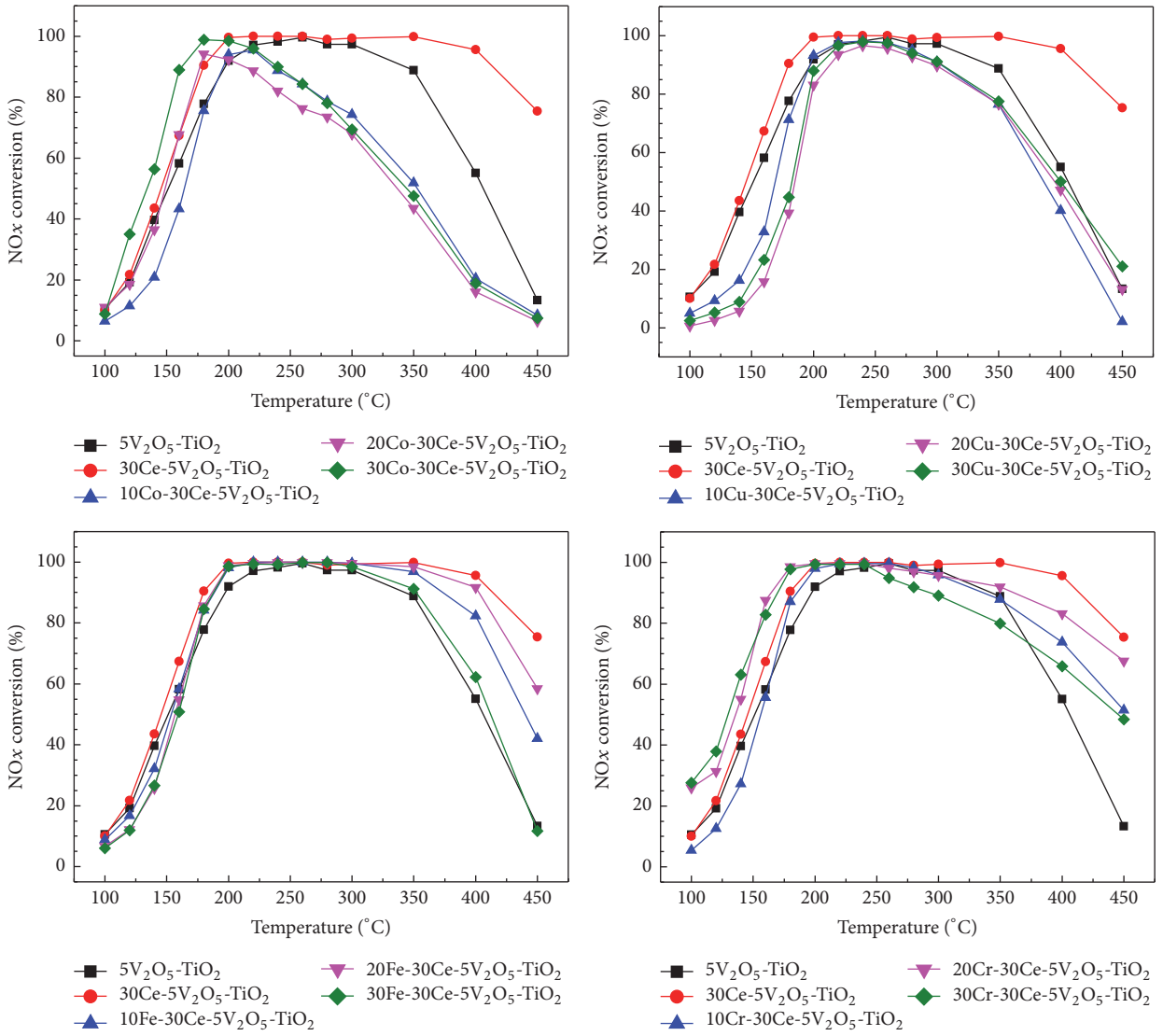

Figure 4: NOx conversion over Co-30Ce, Cu-30Ce, Fe-30Ce, and Cr-30Ce codoped V_2O_5/TiO_2 catalysts with different Co, Cu, Fe, and Cr loading contents.

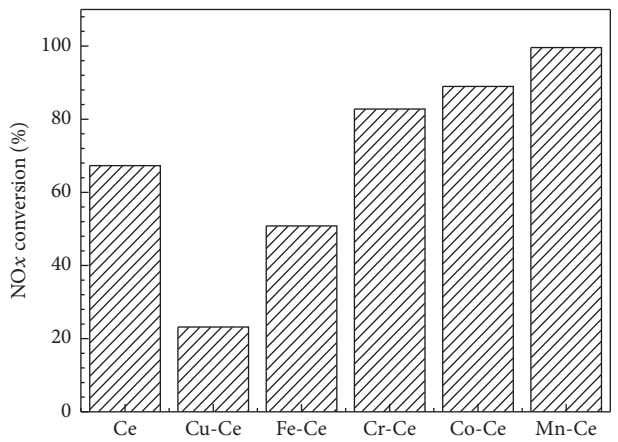

Figure 5: NOx conversion over X-Ce codoped V_2O_5/TiO_2 catalysts with different loading metals at 160°C.

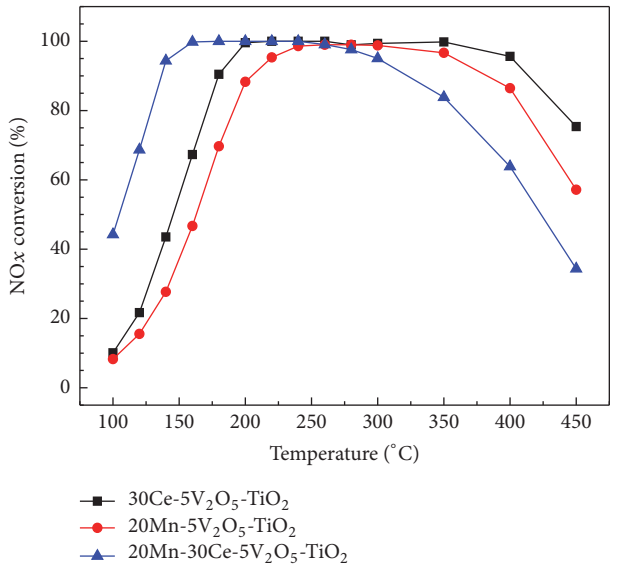

Figure 6: NOx conversion over 20Mn-30Ce-5V_2O_5/TiO_2, 30Ce-5V_2O_5/TiO_2, and 20Mn-5V_2O_5/TiO_2 catalysts.

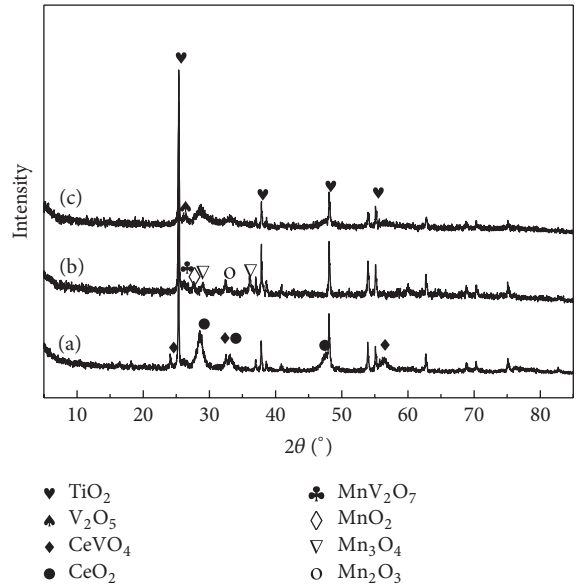

Figure 7: XRD profiles of (a) Ce-doped, (b) Mn-doped, and (c) Mn-Ce codoped V_2O_5/TiO_2 catalysts.

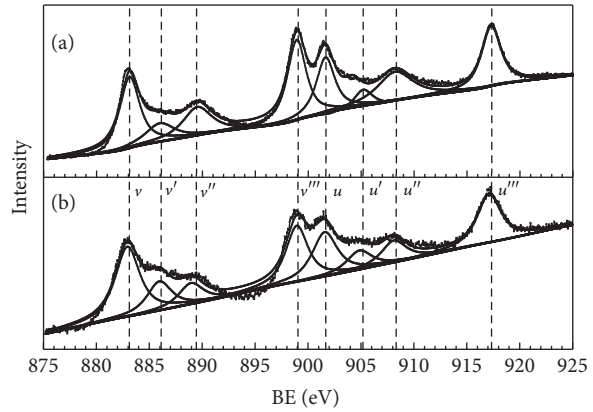

Figure 8: XPS spectra of Ce 3d of (a) Mn-Ce-V_2O_5/TiO_2 (20Mn-30Ce) and (b) Ce-V_2O_5/TiO_2 (30Ce) catalysts.

Table 1: Comparison of BET surface area, pore volume, and average pore diameter.

Samples	BET surface area (m^2/g)	Pore volume (cm^3/g)	Average pore diameter (nm)
V_2O_5-TiO_2	5.5022	0.025621	186.2567
Ce-V_2O_5-TiO_2	28.7009	0.141243	196.8476
Mn-V_2O_5-TiO_2	8.9057	0.061350	271.3350
Mn-Ce-V_2O_5-TiO_2	33.5854	0.125967	150.0261

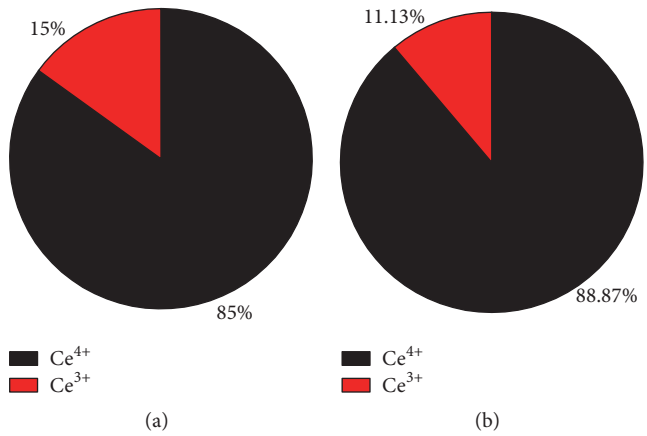

Figure 9: Surface atomic concentration ratio of Ce^{3+} and Ce^{4+}. (a) 30Ce-5V_2O_5/TiO_2 and (b) 20Mn-30Ce-5V_2O_5/TiO_2.

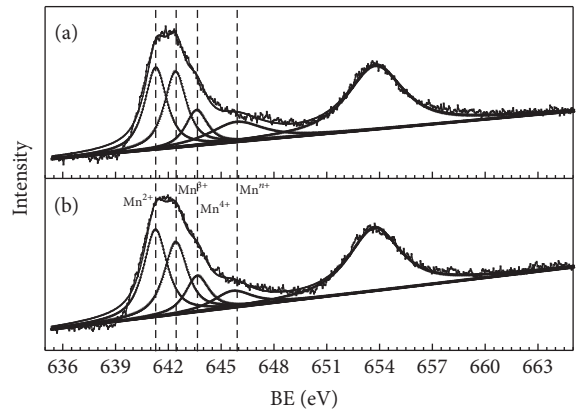

Figure 10: XPS spectra of Mn 2p of (a) Mn-Ce-V_2O_5/TiO_2 (20Mn-30Ce) and (b) Mn-V_2O_5/TiO_2 (20Mn) catalysts.

has two main peaks, Mn 2p1/2 (near 654 eV) and Mn 2p3/2 (near 642 eV), respectively. The characteristic peak of Mn 2p3/2 is superimposed from four peaks of Mn with different valence. Divide the characteristic peak into four subpeaks that Mn^{2+} (641.2–641.5 eV), Mn^{3+} (642.3–642.5 eV), Mn^{4+} (643.5–643.8 eV), and Mn^{n+} (645.8–646.0 eV) can be achieved. The relative surface concentration of Mn^{2+}, Mn^{3+}, and Mn^{4+} calculated by the peak area is shown in Figure 11. Mn mostly exists in the form of Mn^{2+} in both Mn-Ce codoped and single Mn-doped catalyst. The higher the valence, the lower the atomic concentration. Under the interaction in Mn-Ce codoped system, a small part of the low-valence Mn^{2+} is oxidized to Mn^{3+}. The incorporation of Mn can react with Ce which has a variable valence that can promote the electron transfer between active components. Some chemical reactions may occur between the Mn^{2+} and Ce^{4+} as the following:

$$\begin{aligned} Mn^{2+} + Ce^{4+} &\longrightarrow Mn^{3+} + Ce^{3+} \\ 2Ce^{3+} + \frac{1}{2}O_2 &\longrightarrow 2Ce^{4+} + O^{2-} \end{aligned} \quad (3)$$

The XPS spectra of V 2p of Mn-Ce codoped and single Ce- and Mn-doped V_2O_5/TiO_2 catalyst are shown in Figure 12. The characteristic peak of V2p3/2 appears within 515~518 eV, which can be divided into two peaks, V^{4+} (516.7 eV) and V^{5+} (517.6 eV). The relative surface concentration of V^{4+} and V^{5+} calculated by the peak area is shown in Figure 13. The concentration of V^{5+} in a descending order of Mn-Ce codoped > Ce-doped> Mn-doped. V^{5+} is the active center of

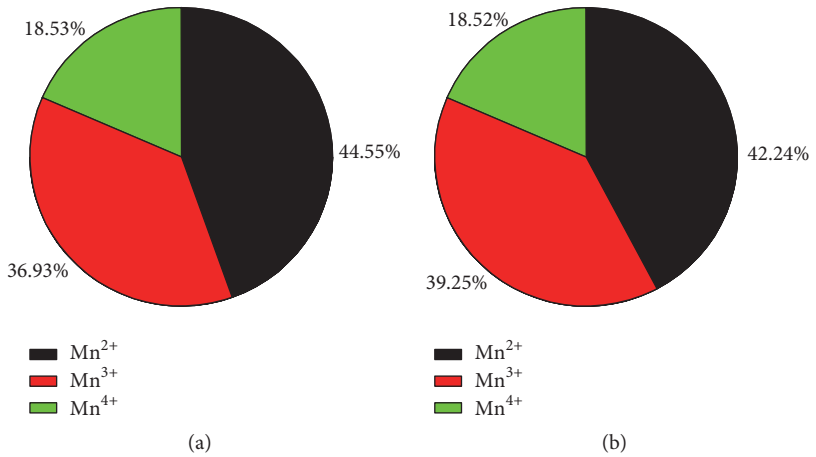

Figure 11: Surface atomic concentration ratio of of Mn^{2+}, Mn^{3+}, and Mn^{4+}. (a) Mn-V_2O_5/TiO_2 and (b) Mn-Ce-V_2O_5/TiO_2.

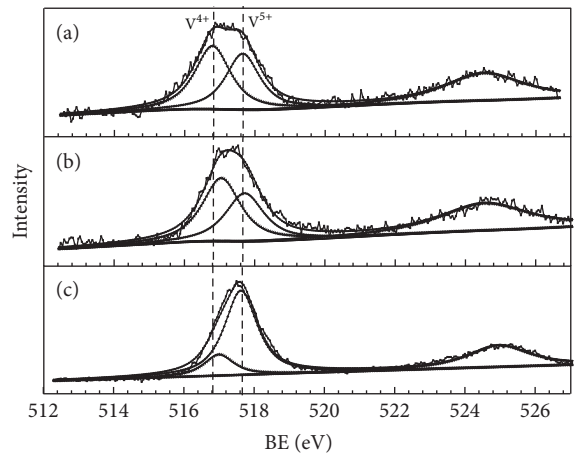

Figure 12: XPS spectra of V 2p of (a) 30Ce-5V_2O_5/TiO_2 (30Ce), (b) 20Mn-5V_2O_5/TiO_2 (20Mn), and (c) 20Mn-30Ce 5V_2O_5/TiO_2 (20Mn-30Ce) catalysts.

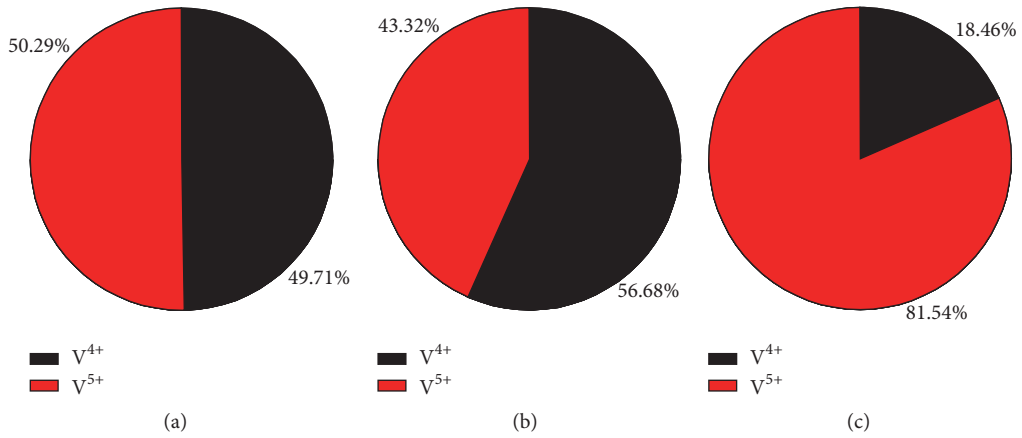

Figure 13: Surface atomic concentration ratio of V^{4+} and V^{5+}. (a) 20Mn-5V_2O_5/TiO_2, (b) 30Ce-5V_2O_5/TiO_2, and (c) 20Mn-30Ce-5V_2O_5/TiO_2.

the denitration catalyst and NO and NH_3 can easily adsorb on the V^{5+} centers that promote the oxidation and reduction of NO. Under the coeffect of Mn and Ce, a lot of V^{4+} convert into more active V^{5+}; the concentration of V^{5+} increased more than 30%.

The XPS results show that the Mn-Ce codoped catalysts promote the interaction among Mn, Ce, and V. The three kinds of atoms are moving to higher valence direction, which is benefical for elcetron transformation and oxidation ability of the whole catalytic system. This is more conducive to the NOx reduced by HN3 at low temperatures.

4. Conclusions

Typical p-type semiconductor MnOx codoped with n-type semiconductors such as CeO_2 and V_2O_5 achieved the excellent effect on NO removal by NH_3. Mn-Ce codoped vanadium-titanium catalyst system can effectively lower the reaction temperature and improve the efficiency. The NOx conversion over Mn-Ce codoped V_2O_5/TiO_2 catalyst can reach more than 90% at 140°C that is much higher than single doped catalyst. Mn-Ce codoped V_2O_5/TiO_2 catalyst has the best low-temperature activity that can drop to 80°C which is lower than single Mn-doped catalyst and Ce-doped catalyst. The codoping of Mn-Ce makes Ce exist in the form of CeO_2, but Mn is mostly in amorphous state on the surface which can achieve better low-temperature effect. The incorporation of Mn can react with Ce which has a variable valence that can promote the electron transfer between the two active components to form an effective electron circulation in the presence of oxygen. The Mn, Ce, and V are moving to higher valence direction that the oxidation increased, which is more conducive to the NO_X reduced by NH_3. Thus even at low temperatures, it is possible to release O radical in the process of NO adsorption, which can be oxidized to NO_2 and then react with NH_3. All in all, Mn-Ce codoped V_2O_5/TiO_2 catalyst utilizes the electron transfer between Mn, Ce, and V effectively, and the denitration performance at low temperature is greatly improved. This finding may help scientists and engineers to development next generation smart surfaces [24, 25] with absorption functionality.

Conflicts of Interest

The authors declare that they have no conflicts of interest.

Authors' Contributions

Quan Xu, Peng Pu, and Li Cao conceived and designed the experiments; Ke Yang and Weiwei Xiao performed the experiments; Jiaojiao Bai, Li Cao, Yan Luo, and Hao Guo analyzed the data; Wei Cai contributed reagents/materials/analysis tools; Peng Pu and Quan Xu wrote the paper.

Acknowledgments

The authors thank Beijing Municipal Science and Technology Project (nos. Z161100001316010 and D141100002814001), National Key Research and Development Plan (no. 2016YFC0303701), Tribology Science Fund of State Key Laboratory of Tribology (no. SKLTKF16A06), and Science Foundation of China University of Petroleum (nos. 2462014YJRC011, ZX20160056, and 201603) for the support.

References

[1] R. M. Heck, "Catalytic abatement of nitrogen oxides–stationary applications," *Catalysis Today*, vol. 53, no. 4, pp. 519–523, 1999.

[2] S. C. Wood, "Select the right IMOx control technology," *Chemical Engineering Progress. Energy Technology Consultants*, p. 33, 1994.

[3] M. F. H. Van Tol, M. A. Quinlan, F. Luck, G. A. Somorjai, and B. E. Nieuwenhuys, "The catalytic reduction of nitric oxide by ammonia over a clean and vanadium oxide-coated platinum foil," *Journal of Catalysis*, vol. 129, no. 1, pp. 186–194, 1991.

[4] L. Chmielarz, P. Kuśtrowski, R. Dziembaj, P. Cool, and E. F. Vansant, "Catalytic performance of various mesoporous silicas modified with copper or iron oxides introduced by different ways in the selective reduction of NO by ammonia," *Applied Catalysis B: Environmental*, vol. 62, no. 3-4, pp. 369–380, 2006.

[5] Q. Li, H. Yang, F. Qiu, and X. Zhang, "Promotional effects of carbon nanotubes on V_2O_5/TiO_2 for NO_X removal," *Journal of Hazardous Materials*, vol. 192, no. 2, pp. 915–921, 2011.

[6] P. S. Metkar, M. P. Harold, and V. Balakotaiah, "Selective catalytic reduction of NOx on combined Fe-and Cu-zeolite monolithic catalysts: sequential and dual layer configurations," *Applied Catalysis B: Environmental*, vol. 111, pp. 67–80, 2012.

[7] X. Wu, Z. Si, G. Li, D. Weng, and Z. Ma, "Effects of cerium and vanadium on the activity and selectivity of MnO_x-TiO_2 catalyst for low-temperature NH3-SCR," *Journal of Rare Earths*, vol. 29, no. 1, pp. 64–68, 2011.

[8] Z. Wu, R. Jin, H. Wang, and Y. Liu, "Effect of ceria doping on SO_2 resistance of Mn/TiO_2 for selective catalytic reduction of NO with NH_3 at low temperature," *Catalysis Communications*, vol. 10, no. 6, pp. 935–939, 2009.

[9] M. Kang, J. Choi, Y. T. Kim et al., "Effects of preparation methods for V_2O_5-TiO_2 aerogel catalysts on the selective catalytic reduction of NO with NH_3," *Korean Journal of Chemical Engineering*, vol. 26, no. 3, pp. 884–889, 2009.

[10] L. Xiong, Q. Zhong, Q. Chen, and S. Zhang, "TiO_2 nanotube-supported V_2O_5 catalysts for selective NO reduction by NH_3," *Korean Journal of Chemical Engineering*, vol. 30, no. 4, pp. 836–841, 2013.

[11] Q. Li, X. Hou, H. Yang et al., "Promotional effect of CeO X for NO reduction over V_2O_5/TiO_2-carbon nanotube composites," *Journal of Molecular Catalysis A: Chemical*, vol. 356, pp. 121–127, 2012.

[12] J. Li, H. Chang, L. Ma, J. Hao, and R. T. Yang, "Low-temperature selective catalytic reduction of NO_x with NH_3 over metal oxide and zeolite catalysts—a review," *Catalysis Today*, vol. 175, no. 1, pp. 147–156, 2011.

[13] J. M. García-Cortés, J. Pérez-Ramírez, M. J. Illán-Gómez, F. Kapteijn, J. A. Moulijn, and C. Salinas-Martínez de Lecea, "Comparative study of Pt-based catalysts on different supports in the low-temperature de-NOx-SCR with propene," *Applied Catalysis B: Environmental*, vol. 30, no. 3-4, pp. 399–408, 2001.

[14] H. Xu, Z. Qu, C. Zong, F. Quan, J. Mei, and N. Yan, "Catalytic oxidation and adsorption of Hg^0 over low-temperature NH_3-SCR $LaMnO_3$ perovskite oxide from flue gas," *Applied Catalysis B: Environmental*, vol. 186, pp. 30–40, 2016.

[15] M. Kang, E. D. Park, J. M. Kim, and J. E. Yie, "Manganese oxide catalysts for NOx reduction with NH_3 at low temperatures," *Applied Catalysis A: General*, vol. 327, no. 2, pp. 261–269, 2007.

[16] M. Wallin, S. Forser, P. Thormählen, and M. Skoglundh, "Screening of TiO_2-supported catalysts for selective NO_x reduction with ammonia," *Industrial & Engineering Chemistry Research*, vol. 43, no. 24, pp. 7723–7731, 2004.

[17] G. Qi and R. T. Yang, "Performance and kinetics study for low-temperature SCR of NO with NH_3 over MnOx–CeO_2 catalyst," *Journal of Catalysis*, vol. 217, no. 2, pp. 434–441, 2003.

[18] W. Shan, F. Liu, Y. Yu, and H. He, "The use of ceria for the selective catalytic reduction of NO_x with NH_3," *Chinese Journal of Catalysis*, vol. 35, no. 8, pp. 1251–1259, 2014.

[19] Z. Wu, B. Jiang, Y. Liu, W. Zhao, and B. Guan, "Experimental study on a low-temperature SCR catalyst based on MnOx/TiO2 prepared by sol-gel method," *Journal of Hazardous Materials*, vol. 145, no. 3, pp. 488–494, 2007.

[20] L. Zhang, Q. Xu, J. Niu, and Z. Xia, "Role of lattice defects in catalytic activities of graphene clusters for fuel cells," *Physical Chemistry Chemical Physics*, vol. 17, no. 26, pp. 16733–16743, 2015.

[21] Q. Xu, Y. Lv, C. Dong et al., "Three-dimensional micro/nanoscale architectures: fabrication and applications," *Nanoscale*, vol. 7, no. 25, pp. 10883–10895, 2015.

[22] J. Liu, L. Yu, Z. Zhao et al., "Potassium-modified molybdenum-containing SBA-15 catalysts for highly efficient production of acetaldehyde and ethylene by the selective oxidation of ethane," *Journal of Catalysis*, vol. 285, no. 1, pp. 134–144, 2012.

[23] Y. Huang, Z.-Q. Tong, B. Wu, and J.-F. Zhang, "Low temperature selective catalytic reduction of NO by ammonia over V_2O_5-CeO_2/TiO_2," *Journal of Fuel Chemistry and Technology*, vol. 36, no. 5, pp. 616–620, 2008.

[24] Y. Wang and X. Gong, "Special oleophobic and hydrophilic surfaces: approaches, mechanisms, and applications," *Journal of Materials Chemistry A*, vol. 5, no. 8, pp. 3759–3773, 2017.

[25] C. Zhang, D. A. Mcadams, and J. C. Grunlan, "Nano/micro-manufacturing of bioinspired materials: a review of methods to mimic natural structures," *Advanced Materials*, vol. 28, no. 30, pp. 6292–6321, 2016.